

# Metal-as-insulation sub-scale prototype tests under a high background magnetic field

Philippe Fazilleau<sup>1</sup> , Benjamin Borgnic<sup>2</sup>, Xavier Chaud<sup>2</sup>, François Debray<sup>2</sup>, Thibault Lécresse<sup>1</sup>  and Jung-Bin Song<sup>2</sup>

<sup>1</sup>CEA, Université Paris-Saclay, 91191 Gif-sur-Yvette, France

<sup>2</sup>CNRS, Laboratoire National des Champs Magnétiques Intenses (LNCMI), Université Grenoble Alpes, 38042 Grenoble, France

E-mail: [philippe.fazilleau@cea.fr](mailto:philippe.fazilleau@cea.fr)

Received 11 May 2018, revised 18 June 2018

Accepted for publication 9 July 2018

Published 30 July 2018



## Abstract

The aim of the NOUGAT project is to design and realize a 10 T high temperature superconducting solenoidal insert able to operate in a 20 T background magnetic induction. Our design is based on the metal-as-insulation winding technique consisting of co-winding a bare REBCO high temperature superconducting tape with a stainless steel tape. The metal-as-insulation winding maintains the self-protection feature of the no insulation winding and helps to reduce current charging time constants—one of the major drawbacks of no insulation coils—by significantly increasing the turn-to-turn electrical resistance. First, we demonstrated the self-quench protective behavior at 4.2 K under a high field up to 17 T by testing a single-pancake prototype. Then, before fabricating the final insert, we designed, wound and tested a second prototype made of two double-pancakes. The purposes were three-fold: validating the winding and assembly process, confirming the operating margins and corroborating the mechanical study. In this article, we present the main results of the tests performed at 4.2 K on this sub-scale prototype in a high background magnetic field at Laboratoire National des Champs Magnétiques Intenses at Grenoble.

Keywords: high field magnets, no insulation winding, metal-as-insulation winding, pancake coil

(Some figures may appear in colour only in the online journal)

## 1. Introduction

The purpose of the French project ANR NOUGAT is to design and realize a 10 T high temperature superconductor (HTS) solenoidal insert intended to operate in a 20 T background field in order to validate high field HTS insert technologies [1]. The association of a 10 T HTS insert coupled with an existing 20 T resistive magnet at Laboratoire National des Champs Magnétiques Intenses at Grenoble (LNCMI-G) is the first step towards a full 30 T HTS user magnet. The geometric constraints are to fit inside the existing cold bore cryostat leaving 128 mm for the prototype outer diameter. The winding inner diameter has been set to 50 mm allowing a cold bore of 38 mm in order for it to be operated as a user magnet.

Since the protection of insulated HTS coils against a quench is particularly difficult, mainly due to the very low propagation velocities of the resistive zone as compared to low temperature superconductors (LTS) [2], we decided to use the metal-as-insulation (MI) winding technique. It consists in co-winding a REBCO HTS tape with a stainless steel tape. The MI winding maintains the self-protection feature of the no insulation (NI) winding [3, 4] and helps to reduce current charging time constants—one of the major drawback of NI coils [5]—by significantly increasing the turn-to-turn electrical resistance [6]. The tests performed on the first prototype demonstrated the self-protective behavior of such winding and the opportunity to manage without a complicated magnet safety system [7].

**Table 1.** SuperPower SCS6050-AP-20 HTS tape main parameters.

Parameter	Unit	Value
Width	mm	6
Total thickness	$\mu\text{m}$	75
Substrate layer thickness	$\mu\text{m}$	50
Superconducting (REBCO) layer thickness	$\mu\text{m}$	1
Silver layer thickness	$\mu\text{m}$	2 (*2)
Copper layer thickness	$\mu\text{m}$	10 (*2)
Critical current at 77 K, self-field ( $I_{c_{tape}}$ )	A	> 210

After this set of tests, we froze the design and decided to test a sub-scale prototype before building the final insert. First, we wanted to validate the winding and assembly process, especially regarding junctions and current leads. Second, we needed to confirm the self-protective behavior and operating margins on a sub-scale prototype. Finally, we had to corroborate the mechanical study as the magnitude of Laplace forces would be high enough at 30 T to irreversibly damage the insert. The MI winding, with its additional stainless steel tape, should withstand such mechanical loadings.

## 2. Experimental set-up

### 2.1. Two MI double-pancake coils

The NOUGAT insert is a 10 T solenoidal coil and the final design is a stack of eight to ten double-pancakes, which allows operating margins in the order of 30% on the load-line.

The sub-scale MI prototype coil is made of two double-pancake coils with the same dimensions as a typical double-pancake designed for the project. Each pancake coil consists of two co-wound tapes: a superconducting tape of the type SCS6050-AP-20 from SuperPower<sup>®</sup> and a Durnomag<sup>®</sup> alloy tape from Laminerie Matthey SA. Both tapes are 6 mm wide and respectively 75  $\mu\text{m}$  and 30  $\mu\text{m}$  thick. The superconducting tape is made of different layers: a 50  $\mu\text{m}$  thick substrate layer made of Hastelloy, a 0.2  $\mu\text{m}$  thick buffer stack layer and a 1  $\mu\text{m}$  thick superconducting layer made of REBCO. It is coated with two 2  $\mu\text{m}$  thick cap layers made of silver. The whole assembly of layers is wrapped with two 10  $\mu\text{m}$  copper layers. The critical current  $I_c$  of a 6 mm tape has a minimal value of 210 A at 77 K in a self-field corresponding to a critical current density  $J_c$  of 467 A mm<sup>-2</sup> in the superconducting tape. These data are listed in table 1.

The pancake coil has 279 turns and about 3 mm of over-banding, i.e. 100 turns of Durnomag<sup>®</sup> alloy. The over-banding purpose is to reduce the global coil deformation, due to Laplace forces, and keep the global HTS tape strain below the limit of 0.4%. G10 insulating foils with a thickness of 300  $\mu\text{m}$  are placed between the pancakes.

The main parameters of the coil are summarized in table 2. The coil should be able to produce between 9 T and 10.3 T with a current of 520 A–590 A in a self-field and between 6.6 T and 7.8 T with a current of 380 A–450 A in a

**Table 2.** MI sub-scale prototype main parameters.

Parameter	Unit	Value
Double-pancake number		2
Winding inner diameter ( $ID_w$ )	mm	50
Winding outer diameter ( $OD_w$ )	mm	109.4
Over-banding thickness ( $t_{ob}$ )	mm	3
Winding turns number ( $n_{bt}$ )		279
Double-pancake critical current at 77 K, self-field ( $I_{c_{coil}}$ )	A	> 60
Coil time constant (measured) <sup>a</sup>	s	5.1
Mutual-inductance between HTS coil and resistive outsert	mH	1.96
Coil characteristics resistance ( $R_c$ ) (calculated)	m $\Omega$	16.3
Average contact surface resistance ( $R_{ct}$ ) <sup>b</sup>	$\mu\Omega \text{ cm}^2$	207
Coil constant ( $\alpha_m$ )	mT A <sup>-1</sup>	17.4
Coil self-inductance ( $L_{HTS}$ )	mH	83
Winding tension	MPa	90–100

<sup>a</sup> The coil time constant is measured from the field delay after the current ramp stop; the internal resistance is obtained from this value and the calculated self-inductance.

<sup>b</sup>  $R_{ct}$  is obtained from  $R_c$  following the formula in [8].

20 T background field ( $B_{ext}$ ). The current redistribution within each tape is considered for higher values as the current is uniform within each tape for the lower ones.

The average contact surface resistance  $R_{ct}$  is obtained from the measurement of the field delay; with 207  $\mu\Omega \text{ cm}^2$  for the MI winding, it is much larger than the usual value measured for NI windings, 20–70  $\mu\Omega \text{ cm}^2$  [5, 8].

Photographs of the two double-pancake coil sample mounted on the probe are shown in figure 1.

### 2.2. LNCMI-G 20 T test facility

The tests of the prototype are performed under a high magnetic background field. The test facility is the LNCMI-G M10 site in its 170 mm room temperature bore configuration. The generation of the field is ensured by resistive magnets which are a combination of poly-helix coils and Bitter stacks [9]. A total power of 18 MW is needed to produce 20 T. Details of the LNCMI-G M10 site are listed in table 3.

The probe is placed in a 128 mm cold bore cryostat that was developed in 2012 for tests at variable temperature [10]. The current leads have been designed to carry up to 1 kA under 20 T. The probe is designed to monitor the sample temperature using CERNOX<sup>®</sup> cryogenic temperature sensors and a 336 Lakeshore temperature controller and to supervise the current lead voltages to avoid thermal runaway.

The DC power supply is a low noise 12 kW (10 V, 1.2 kA) Sorensen SG model from Ametek. The maximal voltage on the sample is about 4 V due to the current lead and cable voltage drop. All signals are recorded through a National Instrument cDAQ-9178 Chassis comprising eight 24-bit modules chosen according to the expected signal ranges (500 mV, 10 V and 60 V). The acquisition of each

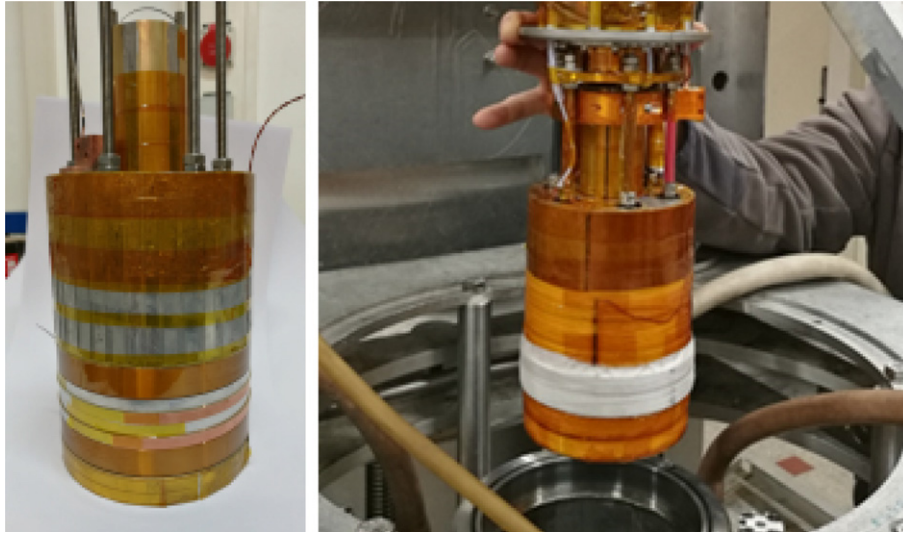


**Figure 1.** Photographs of the sub-scale prototype. Left: before connections and over-banding. Right: during its insertion into the cryostat.

**Table 3.** LNCMI-G M10 site parameters.

Parameter	Unit	Value
Total magnetic induction at center	T	20
Bore diameter	mm	170
Homogeneity in 1 cm <sup>3</sup>	ppm	600
Total power	MW	18
Poly-helix coils		6
Power	MW	7
Magnetic induction	T	10
Bitter stacks		2
Power	MW	11
Magnetic induction	T	10

double-pancake signal and of the assembly is doubled by several 2182A Keithley nano-voltmeters. Protection of the magnet with respect to a quench is ensured by the over-voltage protection of the power supply set between 4 V and 7 V during the test campaign. One of the advantages of using MI winding is that the redistribution of the current in the adjacent turns, when a quench occurs, generates voltages in the order of a volt due to the turn-to-turn resistance. This is larger by more than two to three orders of magnitude compared to the measurement of the resistive zone in an insulated winding, making the protection easier and less subject to noise and fake detections.

### 3. Experimental results

More than 160 tests were performed on the prototype at 4.2 K. The main results are synthesized in figure 2.

The diamond markers represent the maximal magnetic induction and HTS coil power supply current reached for a given external magnetic induction with a stable running experiment without quench. The star markers represent the

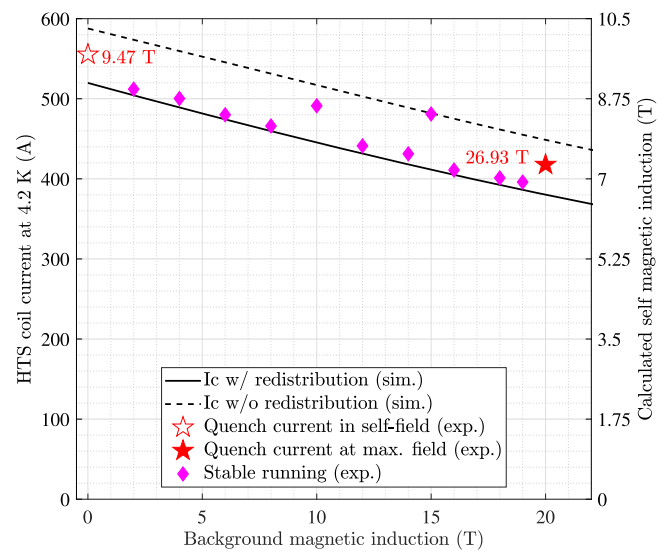


**Figure 2.** Evolution of the central magnetic induction magnitude with respect to the external background magnetic induction.

maximal magnetic induction and HTS coil power supply current reached for a given external magnetic induction with the occurrence of a quench.

The two lines are the limits of the computed critical current of the prototype; they take into account the modulus and orientation of the total magnetic field at each tape [11]. The plain line computation considers that the current density is constant within the tape, making the results more conservative as the current in the tape is then driven by its minimal value. The dashed line computation takes into account the redistribution of the current density within each tape [12]. This assumption leads to a higher critical current and consequently to a higher magnetic induction.

For the tests, we first decided to limit the current to the plain limit (conservative case) in order to have an operating margin and to prevent a quench that could damage the coil.

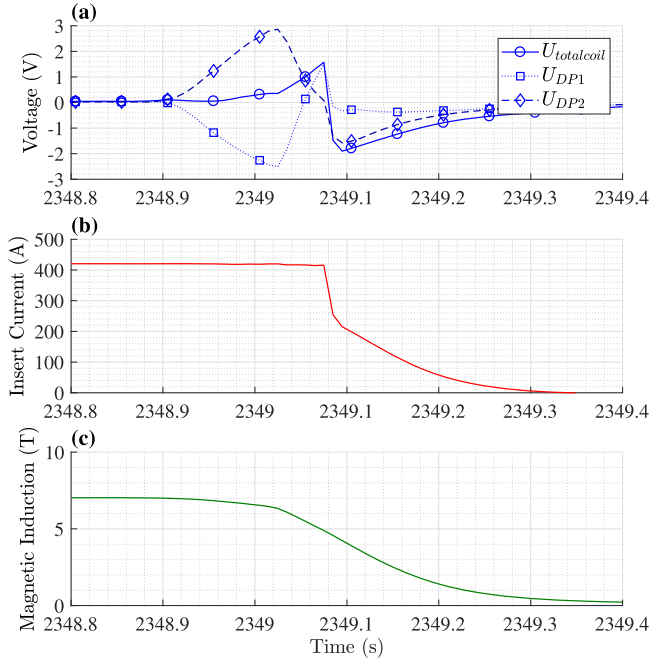


**Figure 3.** Measurements during a quench of the HTS coil at 7 T self-magnetic induction. (a) HTS coil voltages. (b) HTS coil current. (c) Total magnetic induction at the center of the HTS coil.

### 3.1. Self-field test configuration

We first performed tests of the prototype in a self-field configuration with an increasing current. As shown in figure 2, we could reach the conservative limit and decided to increase the current above it; a quench occurred after a plateau of a few seconds at 9.47 T corresponding to 555 A, represented by the empty red star in figure 2.

During these experiments, several quenches occurred due to local heating during current ramping; the coil was perfectly protected thanks to the MI winding and over-voltage protection of the power supply and no damage was visible. For instance, a quench is shown in figure 3. It occurred due to a high ramp rate at 7 T; one can clearly see the self-protective behavior of the MI winding with the decrease of the magnetic field at 2348.9 s prior to the current discharge after 2349.05 s. This is due to the redistribution of the current in the turns adjacent to the resistive zone which leads to a decrease of the ampere-turns and consequently to the magnetic field while the current remains constant. Then, the total voltage at the terminals of the prototype exceeds the protection voltage and the coil is discharged with the power supply. The magnetic induction has already decayed by 30% at the beginning of the current discharge.

At the maximal value of 9.47 T, the total magnetic energy within the sample was 12.8 kJ and the ‘engineering’ current density  $J_e$  within the conductor (including superconducting and stainless steel tapes) and the ‘tape’ current density  $J_t$  (including only the superconducting tape) reached, respectively, 881 A mm<sup>-2</sup> and 1233 A mm<sup>-2</sup>.

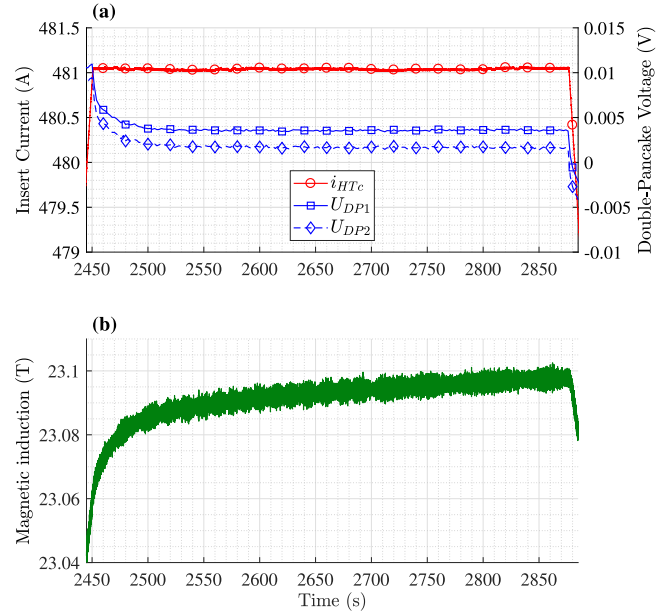


**Figure 4.** Measurements during the plateau at 15 T background magnetic induction. (a) HTS coil current and voltages. (b) Total magnetic induction at the center of the HTS coil.

### 3.2. Background field test configuration

After this first test, we gradually increased the external magnetic field. For each value of the field, we stopped the increase of the current at the conservative limit, as shown in figure 2. No quenches occur below 20 T. Nevertheless, the current ramping rate has to be strongly decreased when approaching the conservative limit due to thermal heating within the coil.

For 10 T, 15 T and 20 T background magnetic inductions, the current was increased above the conservative limit. At 10 T, we stopped the experiment before reaching the second limit of figure 2; the temperature of the liquid helium bath began to increase slowly and continuously and we stopped in order not to take any risk to damage the coil. At 15 T, the same behavior occurred, i.e. a slow increase of the temperature of the bath; the bath pressure was then decreased to stabilize the temperature at 4.2 K and we were able to reach the second limit with a plateau of more than 400 s, as shown in figure 4. While the current of the prototype remained constant during the plateau, the magnetic induction showed a small increase. This is due to the thermally activated flux creep [13] causing a reduction of the screening currents and consequently the homogenization of the current density within the superconducting layer.

A small discrepancy between both double-pancake voltages can be observed; this can be explained by the difference of the value of the internal junction resistance, made by soldering, between the two pancake coils of each double-pancake.

The red plain star in figure 2 gives the value of the maximal current of the prototype reached in the 20 T



background configuration, i.e. 417 A. This corresponds to a self-magnetic induction of 6.93 T and a total magnetic induction of 26.93 T. The current densities  $J_e$  within the winding (superconducting and stainless steel tapes) and  $J_t$  within the superconducting tape alone reach, respectively,  $663 \text{ A mm}^{-2}$  and  $927 \text{ A mm}^{-2}$ . A quench occurred while ramping up the current above this magnetic induction.

The central magnetic induction measured is lower than the calculated one, with a value of 27.3 T. This is due to the screening current effect which lowers the field and degrades its homogeneity [14]. During this test campaign, we tried to reduce the screening currents by applying different loading sequences. ‘Overshoot’ [15] and ‘vortex shaking’ [16] techniques are commonly used. We performed sweep cycles of the background field around its nominal value with a range of 1–2 T with a mix of both techniques. The results on the demagnetization and the reduction of the screening currents were not successful as we did not measure any increase in the central magnetic field.

### 3.3. Mechanical results

Table 4 compares the computed stresses for the sub-scale prototype at 26.93 T and the final insert in its 9 double-pancake configuration at its nominal current, i.e. at its self-induction of 10 T with a background field of 20 T. The computations were performed with CAST3M [17], an in-house finite-element code. Azimuthal and Von Mises stresses have been calculated within each model, considering no impregnation of the winding. The over-banding as described in section 2.1 is taken into account in the computation and the mechanical loadings are the thermal cooling and the Laplace forces.

The ‘JBr’ formula is the well-known simple analytical calculation based on the assumption that each turn acts independently of its neighbors and develops an overall hoop stress  $\sigma_\theta = J B r$ , where  $r$  is the radius of the considered turn,  $J$  its current density and  $B$  the local magnetic induction.

The results show that the prototype is highly constrained at 26.93 T as its stresses exceed 800 MPa and even 900 MPa for the JBr calculation. It should be noted that the advanced computation with CAST3M shows maximum stresses in the inner part of the pancakes while they are obviously in the external one for the JBr calculation. The prototype, only composed of two double-pancakes, generates a self-field of 6.93 T with a background field of 20 T.

In comparison, the final insert at 30 T in its nominal configuration is less constrained with stresses around 500 MPa leaving a large margin with regards to the mechanics. We could expect to reach 34 T in an ultimate scenario, i.e. at the mechanical limit of the materials composing the magnet.

### 3.4. Magnetic coupling with the resistive outsert

The occurrence of the event at 26.93 T was due to a quench of the HTS insert. Figure 5 shows the measurements performed

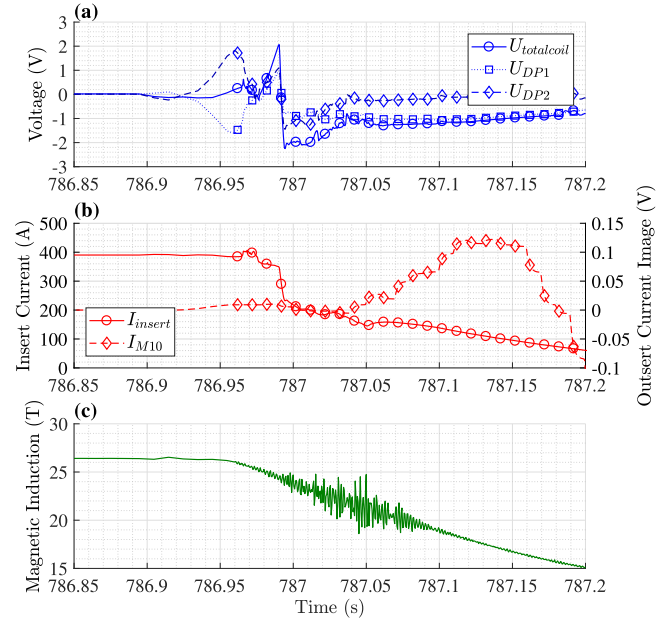


**Figure 5.** Measurements during a quench of the HTS coil followed by the discharge of the resistive outsert at 20 T background magnetic induction. (a) HTS coil voltages. (b) HTS coil current and outsert current image. (c) Total magnetic induction at the center of the HTS coil.

**Table 4.** Mechanical computations.

	Sub-scale prototype	Final NOUGAT insert
Double-pancakes	2	9
$B_{centre}$	26.93 T	30 T
Azimuthal stresses	838 MPa	454 MPa
Von Mises stresses	890 MPa	468 MPa
JBr	916 MPa	523 MPa

during this event. The blue plots correspond to the voltages at the terminals of the two double-pancakes and the terminals of the total coil. The red plots correspond to the current of the HTS insert and the current image of the M10 resistive outsert. For this measurement, the 0 value corresponds to a current image for which the external background field is 20 T. The green plot corresponds to the central magnetic induction.

We can clearly see the development of a quench with the increase of both voltages of the HTS double-pancakes. It should be noted that they increase rapidly to more than 1 V in approximately 50 ms. During this first phase and due to the mutual magnetic coupling between the HTS insert and resistive outsert, the current of the outsert undergoes a slight increase. The magnetic field remains constant. Then, as the quench spreads within the winding, there is a slight increase of the HTS insert current due to the redistribution of the current within the MI winding. The magnetic field starts to decrease as the coil inductance becomes consequently smaller. Finally, the HTS insert discharges with a decrease of the magnetic field and a larger increase of the resistive outsert due to the already mentioned magnetic coupling. This event was

less destructive for the HTS insert than those we measured during the first test campaign when the prototype was quenched consecutively to an unexpected outsert discharge [7]. Measurements performed after this event show that the critical current of the prototype dropped by 8%; after unwinding the coil, the damaged parts were located around the junctions, especially the internal ones where the mechanical stresses are the highest, as shown by the computations.

In order to protect the HTS insert against the outsert discharges, several solutions exist: first, eddy current shielding, used in LTS hybrid magnets [18], can help to smooth the magnetic field discharge, but it is difficult to apply to our coil due to geometric constraints. Second, a protection resistor can be added to the electrical circuit via switch breakers with the occurrence of the outsert discharge. It could help to reduce the current induced in the HTS insert. Moreover, as stated *supra*, the voltages at the terminals of the double-pancakes rapidly reach values in the order of a volt, making the detection easier than in the case of HTS insulated windings.

## 4. Conclusion

The tests performed on the sub-scale prototype provided interesting answers to several technical questions before the fabrication of the final insert.

First, the self-protective behavior of the MI winding has once again been demonstrated with several self-quenches without any degradation of the coil. The current density  $J_c$  reached more than  $850 \text{ A mm}^{-2}$  in a self-field and more than  $650 \text{ A mm}^{-2}$  under 20 T. The issue with such hybrid magnets comes from the coupling between the resistive outsert and HTS insert. The magnetic energy transferred during a disruption of the outsert and its associated Laplace forces can strongly damage the HTS insert, particularly in the junction areas. This is one of the major drawbacks we have to address in the future.

Second, we demonstrate that the technological solutions designed for the final insert, such as internal and external junctions, the over-banding technique and current leads, are reliable. We could operate the prototype under a high magnetic field with a very good current stability over several minutes.

Finally, we were able to reach a total magnetic induction of 26.93 T, composed of 6.93 T generated by the two double-pancake prototype and 20 T from the resistive outsert; the mechanical stresses are very large at this induction value with more than 850 MPa. The final insert in its nominal configuration will be less constrained, with stresses in the order of 500 MPa, giving a margin of more than 45%.


## Acknowledgments

The authors acknowledge the support of the LNCMI-CNRS, member of the European Magnetic Field Laboratory (EMFL), and of the French National Research Agency (ANR) through the contracts ANR-10-LABX-51-01 (Labex LANE—HTS

winding project) and ANR-14-CE05-0005 (project NOUGAT, ‘NOUvelle Génération d’Aimants pour la production de Teslas’).

## ORCID iDs

Philippe Fazilleau  <https://orcid.org/0000-0001-6400-5626>

Thibault Lécrovisse  <https://orcid.org/0000-0001-6516-7600>

## References

- [1] Borgnolutti F, Badel A, Benkel T, Chaud X, Debray F, Fazilleau P, Lécrovisse T and Tixador P 2016 Design study of a 10-T REBCO insert solenoid *IEEE Trans. Appl. Supercond.* **26** 4600405
- [2] Lécrovisse T, Chaud X, Debray F, Devaux M, Fazilleau P, Juster F P, Miyoshi Y, Rey J M, Tixador P and Vincent B 2013 Quench propagation in YBCO pancake: experimental and computational results *IEEE Trans. Appl. Supercond.* **23** 4601805
- [3] Kim K, Kim K, Bhattarai K R, Radcliff K, Jang J Y, Hwang Y J, Lee S G, Yoon S and Hahn S 2017 Quench behavior of a no-insulation coil wound with stainless steel cladding REBCO tape at 4.2 K *Supercond. Sci. Technol.* **30** 075001
- [4] Yoon S, Kim J, Cheon K, Lee H, Hahn S and Moon S-H 2016 26 T 35 mm all-GdBa<sub>2</sub>Cu<sub>3</sub>O<sub>7-x</sub> multi-width no-insulation superconducting magnet *Supercond. Sci. Technol.* **29** 04LT04
- [5] Zhang Z, Kim C H, Kim J G, Kvitkovic J, Pamidi S, Zhang M, Li J and Yuan W 2017 An experimental investigation of the transient response of HTS non-insulation coil *J. Supercond. Novel Magn.* **30** 387–93
- [6] Lécrovisse T and Y Iwasa 2016 A (RE)BCO pancake winding with metal-as-insulation *IEEE Trans. Appl. Supercond.* **26** 4700405
- [7] Lécrovisse T, Badel A, Benkel T, Chaud X, Fazilleau P and Tixador P 2018 Metal-as-insulation variant of no-insulation HTS winding technique: pancake tests under high background magnetic field and high current at 4.2 K *Supercond. Sci. Technol.* **31** 055008
- [8] Wang X, Hahn S, Kim Y, Bascuñán J, Voccio J, Lee H and Iwasa Y 2013 Turn-to-turn contact characteristics for an equivalent circuit model of no-insulation REBCO pancake coil *Supercond. Sci. Technol.* **26** 035012
- [9] Debray F, Dumas J, Trophime C and Vidal N 2012 Dc high field magnets at the LNCMI *IEEE Trans. Appl. Supercond.* **22** 4301804
- [10] Miyoshi Y *et al* 2013 HTS coil test facility in a large bore 20 T resistive magnet at LNCMI *IEEE Trans. Appl. Supercond.* **23** 9500204
- [11] Fleiter J and Ballarino A 2014 Parametrization of the critical surface of REBCO conductors from Fujikura *CERN Technical Report* note 2014-24, EDMS no. 1426239
- [12] Zermeno V, Sirois F, Takayasu M, Vojenciak M, Kario A and Grilli F 2015 A self-consistent model for estimating the critical current of superconducting devices *Supercond. Sci. Technol.* **28** 085004
- [13] Anderson P W and Kim Y B 1964 Hard superconductivity—theory of motion of Abrikosov flux lines *Rev. Mod. Phys.* **36** 39

- [14] Dilasser G, Fazilleau P and Tixador P 2017 Experimental measurement and numerical simulation of the screening current-induced field decay in a small REBCO coil *IEEE Trans. Appl. Supercond.* **27** 4900104
- [15] Yanagisawa Y, Kominato Y, Nakagome H, Fukuda T, Takematsu T, Takao T, Takahashi M and Maeda H 2012 Effect of coil current sweep cycle and temperature change cycle on the screening current-induced magnetic field for YBCO-coated conductor coils *AIP Conf. Proc.* **1434** 1373–80
- [16] Brandt E H and Mikitik G P 2003 Shaking of the critical state by a small transverse ac field can cause rapid relaxation in superconductors *Supercond. Sci. Technol.* **17** S1
- [17] Verpaux P, Charras T and Millard A 1988 Castem 2000 une approche moderne du calcul des structures *Calcul des Structures et Intelligence Artificielle* 261–71
- [18] Fazilleau P, Aubert G, Berriaud C, Hervieu B and Pagnat P 2016 Role and impact of the eddy current shield in the LNCMI-G hybrid magnet *IEEE Trans. Appl. Supercond.* **26** 4301305